Germline P Granules Are Liquid Droplets That Localize by Controlled Dissolution/Condensation

Clifford P. Brangwynne, *et al.*

Science **324**, 1729 (2009);
DOI: 10.1126/science.1172046

Science (print ISSN 0036-8075; online ISSN 1095-9203) is published weekly, except the last week in December, by the American Association for the Advancement of Science, 1200 New York Avenue NW, Washington, DC 20005.

distances. These NMR restraints were also supplemented by a limited number of intersubunit inter-residue distance restraints derived from disulfide mapping measurements that used single-cysteine mutant forms of DAGK. Care was taken to avoid possible motional complications to the disulfide mapping–derived distances. The structure was calculated using standard restrained molecular dynamics and simulated annealing protocols.

15. K. Oxenoid, J. J. Chou, *Proc. Natl. Acad. Sci. U.S.A.* **102**, 10870 (2005).
16. Y. Zhou *et al.*, *Mol. Cell* **31**, 896 (2008).
17. M. Bayrhuber *et al.*, *Proc. Natl. Acad. Sci. U.S.A.* **105**, 15370 (2008).
18. S. Hiller *et al.*, *Science* **321**, 1206 (2008).
19. B. Liang, L. K. Tamm, *Proc. Natl. Acad. Sci. U.S.A.* **104**, 16140 (2007).
20. D. Ma *et al.*, *Proc. Natl. Acad. Sci. U.S.A.* **105**, 16537 (2008).
21. K. A. Baker, C. Tzitzilonis, W. Kwiatkowski, S. Choe, R. Riek, *Nat. Struct. Mol. Biol.* **14**, 1089 (2007).
22. J. H. Chill, J. M. Louis, C. Miller, A. Bax, *Protein Sci.* **15**, 684 (2006).
23. D. J. Miller, A. Jerga, C. O. Rock, S. W. White, *Structure* **16**, 1036 (2008).
24. J. K. Nagy, F. W. Lau, J. U. Bowie, C. R. Sanders, *Biochemistry* **39**, 4154 (2000).
25. A. W. Partridge, R. A. Melnyk, D. Yang, J. U. Bowie, C. M. Deber, *J. Biol. Chem.* **278**, 22056 (2003).
26. J. P. Walsh, L. Fahrner, R. M. Bell, *J. Biol. Chem.* **265**, 4374 (1990).
27. R. E. Bishop, *Biochim. Biophys. Acta* **1778**, 1881 (2008).
28. M. K. Lemberg, M. Freeman, *Mol. Cell* **28**, 930 (2007).
29. D. Martinez Molina *et al.*, *Nature* **448**, 613 (2007).
30. H. J. Snijder *et al.*, *Nature* **401**, 717 (1999).
31. S. Kumar, B. Ma, C. J. Tsai, H. Wolfson, R. Nussinov, *Cell Biochem. Biophys.* **31**, 141 (1999).
32. J. Wen, X. Chen, J. U. Bowie, *Nat. Struct. Biol.* **3**, 141 (1996).
33. H. R. Kaback, M. Sahin-Toth, A. B. Weinglass, *Nat. Rev. Mol. Cell Biol.* **2**, 610 (2001).
34. N. Nagano, C. A. Orengo, J. M. Thornton, *J. Mol. Biol.* **321**, 741 (2002).
35. Single-letter abbreviations for amino acid residues: A, Ala; C, Cys; D, Asp; E, Glu; F, Phe; G, Gly; H, His; I, Ile; K, Lys; L, Leu; M, Met; N, Asn; P, Pro; Q, Gln; R, Arg; S, Ser; T, Thr; V, Val; W, Trp; Y, Tyr.
36. K. Oxenoid, H. J. Kim, J. Jacob, F. D. Sonnichsen, C. R. Sanders, *J. Am. Chem. Soc.* **126**, 5048 (2004).

37. We thank J. Bowie for providing the DAGK expression system, many of the mutants used in this work, and much discussion; M. Voehler, B. Gorzelle, P. Power, C. Kang, and J. Jacob for technical assistance; and K. Oxenoid, L. Kay, S. Prosser, M.-D. Tsai, T. Iverson, J. Meiler, A. Forster, J. Battiste, W. Chazin, and members of the Sanders lab for discussion. Supported by NIH training grant T32 NS007491 (W.V.H.) and National Institute of General Medical Sciences grant RO1 GM47485. C.R.S. is a consultant for Anatrace Inc. (now owned by Affymetrix), a company that markets high-purity biological detergents, including some of the detergents used in sample preparation in this work. The coordinates for DAGK have been deposited as PDB entry 2kdc in the Protein Data Bank. This work is dedicated to the fond memory of Anne Karpay.

Supporting Online Material

www.sciencemag.org/cgi/content/full/324/5935/1726/DC1
Materials and Methods
Figs. S1 to S8
Tables S1 to S4
References

2 February 2009; accepted 7 May 2009
10.1126/science.1171716

Germline P Granules Are Liquid Droplets That Localize by Controlled Dissolution/Condensation

Clifford P. Brangwynne,[1,2,3] Christian R. Eckmann,[1] David S. Courson,[3] Agata Rybarska,[1] Carsten Hoege,[1] Jöbin Gharakhani,[2,3] Frank Jülicher,[2,3] Anthony A. Hyman[1,3]*

In sexually reproducing organisms, embryos specify germ cells, which ultimately generate sperm and eggs. In *Caenorhabditis elegans*, the first germ cell is established when RNA and protein-rich P granules localize to the posterior of the one-cell embryo. Localization of P granules and their physical nature remain poorly understood. Here we show that P granules exhibit liquid-like behaviors, including fusion, dripping, and wetting, which we used to estimate their viscosity and surface tension. As with other liquids, P granules rapidly dissolved and condensed. Localization occurred by a biased increase in P granule condensation at the posterior. This process reflects a classic phase transition, in which polarity proteins vary the condensation point across the cell. Such phase transitions may represent a fundamental physicochemical mechanism for structuring the cytoplasm.

Starting from the fertilized egg, the cells of a developing embryo differentiate to give rise to somatic tissues, as well as maintaining an immortal germ line that will generate sperm and oocytes. Germ-cell specification is mediated in part by ribonucleoprotein granules assembled from RNA and RNA-binding proteins, although the precise function of these granules remains unknown (*1*, *2*). In *Caenorhabditis elegans*, the germ granules are called P granules. P granules are initially distributed uniformly throughout the unpolarized one-cell embryo. Upon symmetry breaking, the embryo polarizes along the anterior-posterior (AP) axis: Cortical and cytoplasmic flows develop (*3*), the polarity proteins PAR-1 and PAR-2 appear on the posterior cortex, and P granules become localized to the posterior half of the cell (Fig. 1A and movie S1; all embryos are ~50 μm long); the embryo then divides, giving rise to a P granule–containing progenitor germ cell and a non–P granule–containing somatic sister cell. Two processes have been proposed to mediate this posterior localization: (i) P granule migration by cytoplasmic flow (*4*–*6*) and (ii) subsequent disassembly or degradation of remaining anterior P granules (*5*–*8*). However, evidence supporting either of these mechanisms is sparse.

To study P granule localization in the one-cell embryo, we used three-dimensional (3D) particle tracking to monitor the movement and fluorescence levels of P granules labeled with green fluorescent protein (GFP)–tagged PGL-1 (*9*, *10*) or GLH-1 (*9*, *11*), both constitutive P granule components. We found that some P granules move into the embryo posterior; however, close to the cortex there was a flux of P granules into the anterior that was of similar magnitude to the posteriorly directed flux (Fig. 1, D to F). This behavior closely matched the overall flow behavior of cytoplasmic material such as yolk granules (*6*), quantified by particle imaging velocimetry (PIV) (Fig. 1, B and C) (*9*). P granules cannot preferentially localize to the posterior by convection in the surrounding cytoplasm alone. Thus, flows have little or no role in P granule localization (*9*).

We next examined intensity changes of individual P granules during localization. We found that P granule size is spatiotemporally controlled (Fig. 2A). We determined the average rate of relative intensity change of a population of P granules, ξ, at different points in space and time (*9*); negative ξ indicates P granule dissolution (i.e., shrinkage) and positive ξ indicates P granule condensation (i.e., growth). Before symmetry breaking, ξ was negative across the entire embryo, indicating overall P granule dissolution (fig. S1). After the onset of symmetry breaking, ξ stayed negative in the anterior but became positive in the posterior of the embryo, indicating posterior condensation [Fig. 2, B (WT, wild type) and C]. As predicted from this analysis, if we delayed symmetry breaking using RNA interference (RNAi) to deplete the centrosomal protein SPD-5 (*12*), ξ stayed negative across the whole embryo, and P granules appeared to dissolve completely [Fig. 2B, *spd-5(RNAi)*]. When these embryos eventually broke symmetry, P granules appeared to form de novo, in the vicinity of posterior PAR proteins (Fig. 2D and figs. S5 and S6). This occurred concomitant with a depletion of soluble P granule components from the anterior cytoplasm (Fig. 2E), and in the absence of notable cytoplasmic flows (movie S3). As with WT embryos, the rate of P granule condensation peaked before leveling off. The maximum of the posterior growth rate in *spd-5(RNAi)* embryos was three times as high as that in WT embryos, which

[1]Max Planck Institute for Molecular Cell Biology and Genetics, 01307 Dresden, Germany. [2]Max Planck Institute for the Physics of Complex Systems, 01187 Dresden, Germany. [3]Marine Biological Laboratory, Woods Hole, MA 02543, USA.

*To whom correspondence should be addressed. E-mail: hyman@mpi-cbg.de

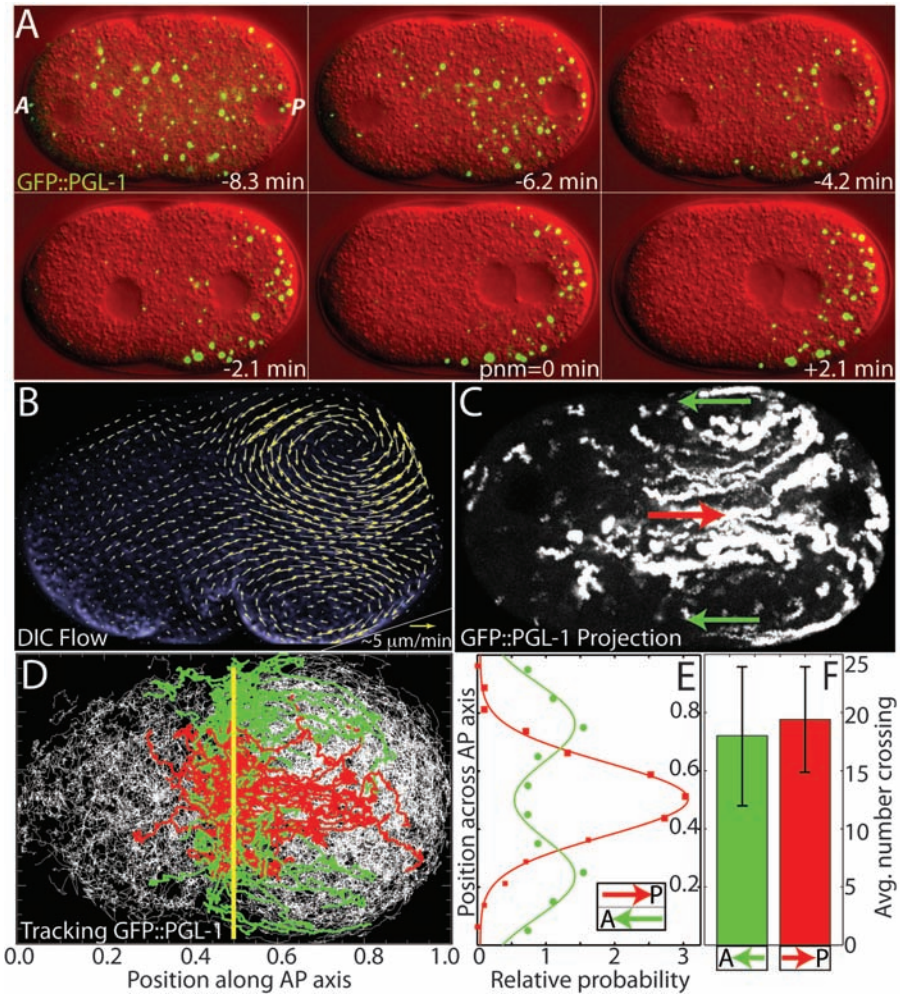

Fig. 1. P granule localization is not due to cytoplasmic flow. (**A**) Fluorescent images of GFP::PGL-1 (green) superimposed on differential interference contrast (DIC) (red). Time relative to pronuclear meeting (pnm). A, anterior; P, posterior. (**B** and **C**) The movement of P granules is similar to the movement of yolk granules. (B) Cytoplasmic flow field from PIV analysis of a single embryo (blue DIC image) during symmetry breaking. Yellow arrows indicate flow direction and magnitude. (C) Maximum-intensity projection of confocal stacks of GFP::PGL-1 P granules in the one-cell embryo during symmetry breaking; first frame, –8 min, 7 s pnm; last frame, –3 min, 30 s pnm; P granules in center of embryo move posteriorly (red arrow), and P granules near cortex move anteriorly (green arrows). (**D**) Overlay of P granule trajectories (white) from five GFP::PGL-1 embryos. Trajectories crossing into the posterior are shown in red, and those crossing into the anterior are in green. (**E**) Probability distribution of the location perpendicular to the AP axis of P granules crossing the midpoint [yellow line in (D)] into anterior (green) versus posterior (red). (**F**) The average flux per embryo (mean ± SEM, $n = 5$) indicates negligible net flux.

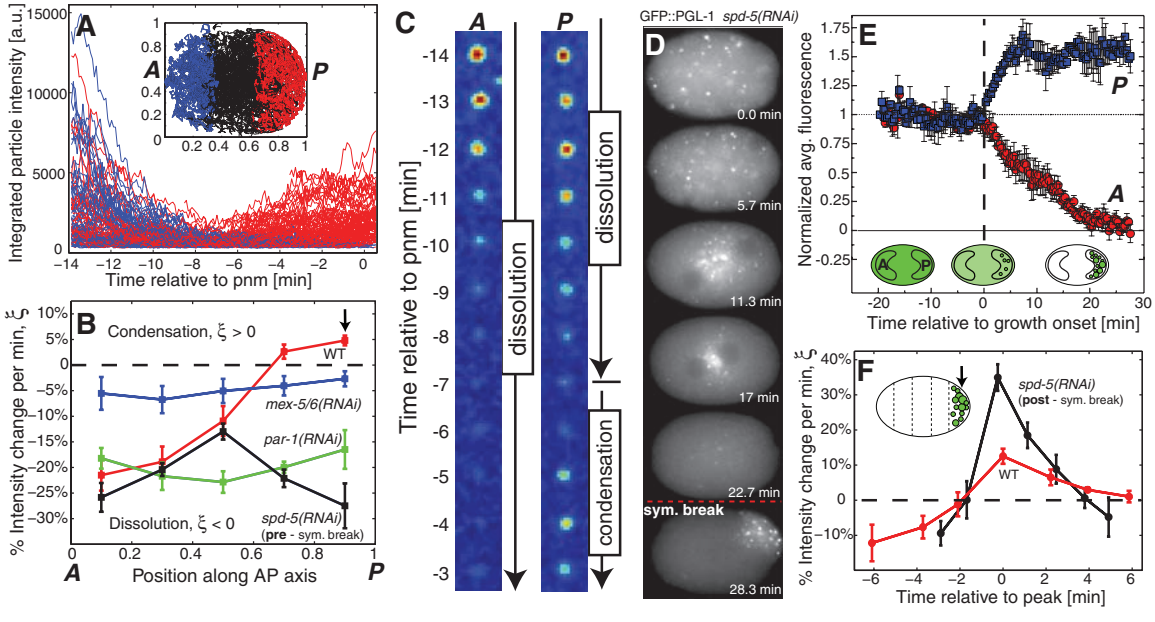

Fig. 2. Spatiotemporal changes in P granule size. (**A**) P granules throughout the one-cell embryo are initially dissolving; blue and red traces are intensities of individual GFP::PGL-1–labeled P granules in the anterior and posterior, respectively. Trajectories in the middle (black) are omitted for clarity. (**B**) *mex-5(RNAi)* ($n = 5$ embryos, blue curve) abrogates the anterior dissolution seen in WT GFP::PGL-1 embryos ($n = 8$, red curve), whereas *par-1(RNAi)* ($n = 6$, green curve) gives rise to dissolution throughout the embryo, as with *spd-5(RNAi)* embryos before symmetry breaking ($n = 8$, black curve). Data are shown as the mean ± SEM. (**C**) Example anterior (A) and posterior (P) GFP::PGL-1–labeled P granule (each recentered), showing anterior dissolution, and posterior dissolution followed by condensation. (**D**) Time sequence of GFP::PGL-1 embryo treated with *spd-5(RNAi)* for >24 hours to delay symmetry breaking. P granules completely dissolve, but then re-form upon symmetry breaking. (**E**) Fluorescence intensity in anterior (A) versus posterior (P) regions of a confocal slice through the middle of the embryo, after complete P granule dissolution in *spd-5(RNAi)* GFP::PGL-1 embryos. Regions of measurements indicated (mean ± SEM, $n = 8$). (**F**) The growth rate of P granules in the embryo posterior (arrow).

may reflect a higher concentration of soluble components due to complete dissolution (Fig. 2F) (*9*). These observations suggest a localization mechanism in which the condensation point is lowered in the posterior, causing condensation of components released by dissolved anterior P granules (see below).

A clue to the molecular control of this behavior comes from the proteins MEX-5 and PAR-1, which are implicated in the degradation of P granule components and P granule stability (*6*–*8*). The MEX-5 concentration is high throughout the embryo before symmetry breaking (*13*, *14*), when we found negative values of ξ across the AP axis [Fig. 2B, *spd-5(RNAi)*]. Upon symmetry breaking, PAR-1 reduces the concentration of MEX-5 in the posterior (*13*–*15*); the resulting MEX-5 concentration gradient was opposite to the dissolution/condensation gradient, ξ (fig. S3). Thus, high MEX-5 levels correlate in space and time with P granule dissolution. Consistent with this, when we depleted embryos of MEX-5, the value of ξ approached zero across the embryo, indicating weakened P granule dissolution [Fig. 2B, *mex-5/6(RNAi)*]. In embryos depleted of PAR-1, which have uniform, high levels of MEX-5 (*13*–*15*), the value of ξ was strongly negative across the AP axis [Fig. 2B, *par-1(RNAi)*], and P granules dissolved throughout (*6*) (movie S6). Thus, PAR-1 and MEX-5 may localize P granules mainly by controlling their dissolution and condensation, rather than by spatially regulating degradation.

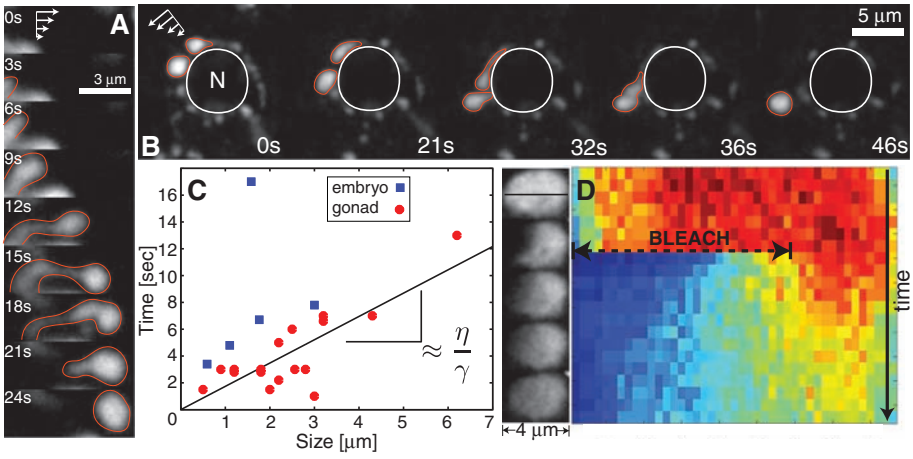

Fig. 3. P granules behave like liquids. (**A**) Jetting P granule (red outline) from a dissected GFP::PGL-1 germline nucleus (lower left, not visible). Shear direction, white arrows. (**B**) Dripping P granules (red outline) from a dissected GFP::PGL-1 germ line. Nucleus (N), white line. (**C**) Time scale of drop breakup and fusion events in dissected germline and early embryos, as a function of droplet size. The black line is a linear fit, yielding a ratio of viscosity to surface tension (η/γ) ≈ 2 s/μm. (**D**) Fluorescence recovery after photobleaching (FRAP) of a large nuclear-associated GFP::PGL-1–labeled P granule from an eight-cell embryo (upper left sequence; top to bottom = 20 s). Kymograph is along the black line in left sequence. Red denotes high intensity and blue, background intensity. The intensity decreases in the unbleached region (fluorescence loss in photobleaching, FLIP) as the bleached region recovers. From exponential fits, in the bleached region τ_{FRAP} = 4.7 s, and in the unbleached region τ_{FLIP} = 5.7 s.

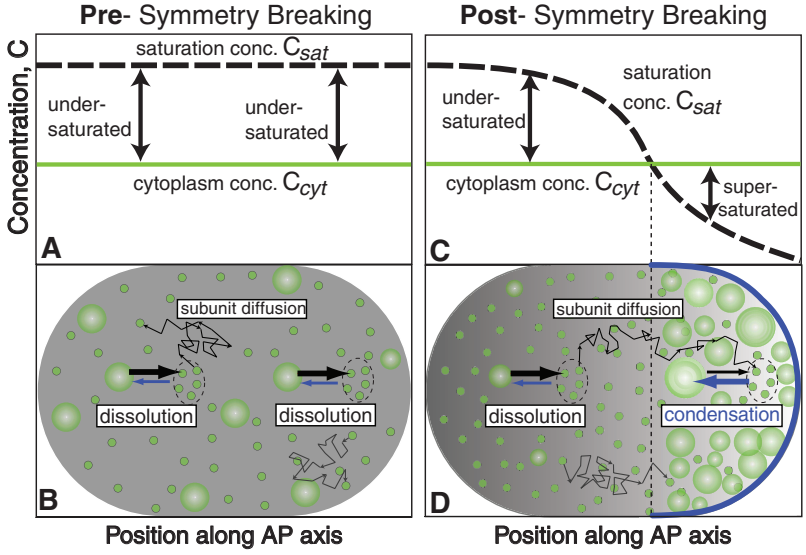

Fig. 4. Proposed mechanism of P granule localization. (**A**) Concentration of soluble components versus position along AP axis (posterior to right). Before symmetry breaking, the condensation point C_{sat} (dashed black line) is high across the embryo. The cytoplasmic concentration of P granule components C_{cyt} (green line) is much lower than C_{sat}, and the embryo is undersaturated with P granule components everywhere. (**B**) Undersaturation leads to dissolution of P granules (large green spheres) into diffusing components (small green circles). (**C**) Symmetry breaking decreases C_{sat} in the posterior, below C_{cyt}. (**D**) Consequently, posterior P granules condense from soluble components, whereas anterior P granules continue dissolving. The spatial dependence of C_{sat} arises from gradients in polarity proteins, including MEX-5 (gray) and PAR-1 (blue).

Our results thus far imply that localization of P granules depends on the ability of subunits to transition between a soluble form and a condensed phase, which appears to be spherical. P granules became nonspherical when they reattached to the nucleus at the four-cell stage, when they appeared similar to liquid drops wetting a surface (fig. S8 and movie S9). Together with the observation that P granules occasionally fused with one another, this suggests that the protein/RNA mixture comprising P granules may behave as a liquid. Indeed, the modularity and weak RNA affinity exhibited by RNA-binding proteins (*16*) would enable rapid molecular rearrangements that could give rise to liquid-like behavior.

For a simple liquid (e.g., water), applied shear stresses induce flows, unlike an elastic solid, which maintains a constant deformed shape under stress (*17*). We induced shear stresses across the large nuclear-associated P granules within the tube-like worm gonad (fig. S2) (*9*). P granules flowed off nuclei, dripped, and often fused into one larger drop; these are classic liquid behaviors (Fig. 3, A and B, and movies S7 to S9). Germ granules in zebrafish may show similar behaviors (*18*).

Liquids exhibit such flow behavior owing to fast internal molecular rearrangements. Consistent with this, when we selectively bleached half of large GFP::PGL-1 P granules at the eight-cell stage, we observed fluorescence recovery on a rapid time scale, τ = 5.9 ± 0.6 s (SEM, n = 5 GFP::PGL-1 P granules); concomitantly, the adjacent unbleached region decreased in fluorescence intensity, suggesting rapid diffusion within the granule (Fig. 3D). Similar observations were made with GFP::GLH-1 embryos (movie S12). Using the length scale of these large granules, L ~ 4 μm, we obtained a diffusion coefficient on the order of $D \sim L^2/\tau \sim$ 1 μm^2/s. By making the simplifying assumption that they behave as equilibrium Newtonian liquids, we could use the Stokes-Einstein relation to obtain a rough estimate of P granule viscosity, η ≈ 1 Pa·s (*9*). This is ~1000 times as large as the viscosity of water, similar to that of glycerol, and comparable to values seen in

colloidal liquids (*19*). Bleaching experiments in early one-cell embryos revealed that components of these P granules (≤1 μm diameter) typically turned over in less than 30 s (fig. S7), suggesting that P granule droplets exist in dynamic equilibrium with soluble components, much as conventional liquids do.

Surface tension is another important parameter controlling the behavior of liquid drops. To quantify P granule surface tension, we measured the time scale of P granules undergoing both fusion and droplet breakup events (Fig. 3, A and B). This time scale increased approximately linearly with the droplet size, as expected for liquids (Fig. 3C). The slope of this line establishes the ratio of viscosity to surface tension, η/γ (*9*). Thus, together with our estimate of P granule viscosity ($\eta \approx 1$ Pa·s), we could make an order of magnitude estimate of the surface tension, γ, between P granules and the cytoplasm, $\gamma \sim 1$ μN/m, which is smaller than the air-water surface tension by a factor of $\sim 10^5$. Such small values are expected for macromolecular liquids (*9*); for example, colloidal liquids typically have $\gamma \sim 0.1$ μN/m and below (*19*, *20*). The surface energetic barrier to P granule formation thus should be small, which may explain their ability to rapidly form upon symmetry breaking (*9*).

The dissolution and condensation behavior we observed, together with the liquid-like nature of P granules, supports a simple physical picture for P granule localization based on the theory of demixing phase transitions in fluids (*21*). Before symmetry breaking, the concentration at which soluble P granule components are saturated, C_{sat}, is uniform and high; the concentration of soluble P granule components, C_{cyt}, is lower than this; P granules are thus undersaturated, causing dissolution throughout the embryo, similar to evaporation of water droplets at high temperature (Fig. 4, A and B). Symmetry breaking causes the posterior value of C_{sat} to decrease below C_{cyt}, and the posterior becomes supersaturated with P granule components; thus, P granule droplets begin condensing, much as air becomes supersaturated with water vapor as temperature is decreased, and water droplets condense. This posterior condensation occurs even while the anterior remains undersaturated, and anterior P granules continue dissolving. This gives rise to a diffusive flux of P granule components into the posterior, thereby clearing out anterior components. The gradient in the condensation point, C_{sat}, along the AP axis appears to be set by gradients in polarity proteins, including MEX-5 and PAR-1 (Fig. 4, C and D). Although protein degradation may also play a role, it appears here that polarity proteins function largely by spatially regulating the P granule "dew point."

We propose that P granule localization exemplifies a general mechanism for organizing the cytoplasm that arises from collections of weakly "sticky" molecules, including other ribonucleoprotein assemblies (e.g., P bodies, Cajal bodies, or stress granules) (*16*, *22*). Such phase structuring may represent a primordial mechanism for functional self-assembly of relatively unevolved molecular assemblies in the early stages of the evolution of life.

References and Notes

1. G. Seydoux, R. E. Braun, *Cell* **127**, 891 (2006).
2. S. Strome, R. Lehmann, *Science* **316**, 392 (2007).
3. S. Q. Schneider, B. Bowerman, *Annu. Rev. Genet.* **37**, 221 (2003).
4. S. N. Hird, J. G. White, *J. Cell Biol.* **121**, 1343 (1993).
5. S. N. Hird, J. E. Paulsen, S. Strome, *Development* **122**, 1303 (1996).
6. R. J. Cheeks *et al.*, *Curr. Biol.* **14**, 851 (2004).
7. C. DeRenzo, K. J. Reese, G. Seydoux, *Nature* **424**, 685 (2003).
8. C. A. Spike, S. Strome, *Curr. Biol.* **13**, R837 (2003).
9. See supporting material on *Science* Online.
10. I. Kawasaki *et al.*, *Cell* **94**, 635 (1998).
11. M. E. Gruidl *et al.*, *Proc. Natl. Acad. Sci. U.S.A.* **93**, 13837 (1996).
12. D. R. Hamill, A. F. Severson, J. C. Carter, B. Bowerman, *Dev. Cell* **3**, 673 (2002).
13. J. R. Tenlen, J. N. Molk, N. London, B. D. Page, J. R. Priess, *Development* **135**, 3665 (2008).
14. A. A. Cuenca, A. Schetter, D. Aceto, K. Kemphues, G. Seydoux, *Development* **130**, 1255 (2003).
15. C. Schubert, R. Lin, C. de Vries, R. Plasterk, J. Priess, *Mol. Cell* **5**, 671 (2000).
16. B. M. Lunde, C. Moore, G. Varani, *Nat. Rev. Mol. Cell Biol.* **8**, 479 (2007).
17. K. E. Kasza *et al.*, *Curr. Opin. Cell Biol.* **19**, 101 (2007).
18. M. J. Strasser *et al.*, *BMC Dev. Biol.* **8**, 58 (2008).
19. D. G. Aarts, M. Schmidt, H. N. Lekkerkerker, *Science* **304**, 847 (2004).
20. M. Daoud, C. E. Williams, S. N. Lyle, Eds., *Soft Matter Physics* (Springer, Berlin, 1999).
21. J. D. Gunton, M. S. Miguel, P. S. Sahni, in *Phase Transitions and Critical Phenomena,* C. Domb, M. S. Green, Eds. (Academic Press, London, 1983), vol. 8.
22. P. Anderson, N. Kedersha, *J. Cell Biol.* **172**, 803 (2006).

23. We thank T. Mitchison for advice and discussion, together with students of the MBL Physiology Course 2008; and S. Grill, N. Goehring, and members of the Hyman and Eckmann Laboratories for helpful comments. We thank S. Hell, R. Medda, and B. Harke for assistance with stimulated emission depletion microscopy. Some strains used in this study were obtained from the Caenorhabditis Genetics Center. C.P.B. is supported by a fellowship from the Helen Hay Whitney Foundation.

Supporting Online Material

www.sciencemag.org/cgi/content/full/1172046/DC1
Materials and Methods
SOM Text
Figs. S1 to S8
References
Movies S1 to S12

9 February 2009; accepted 8 May 2009
Published online 21 May 2009;
10.1126/science.1172046
Include this information when citing this paper.

Ventral Tegmental Area BDNF Induces an Opiate-Dependent–Like Reward State in Naïve Rats

Hector Vargas-Perez,[1]* Ryan Ting-A Kee,[2] Christine H. Walton,[3] D. Micah Hansen,[3] Rozita Razavi,[1] Laura Clarke,[2] Mary Rose Bufalino,[2] David W. Allison,[3] Scott C. Steffensen,[3] Derek van der Kooy[1,2]

The neural mechanisms underlying the transition from a drug-nondependent to a drug-dependent state remain elusive. Chronic exposure to drugs has been shown to increase brain-derived neurotrophic factor (BDNF) levels in ventral tegmental area (VTA) neurons. BDNF infusions into the VTA potentiate several behavioral effects of drugs, including psychomotor sensitization and cue-induced drug seeking. We found that a single infusion of BDNF into the VTA promotes a shift from a dopamine-independent to a dopamine-dependent opiate reward system, identical to that seen when an opiate-naïve rat becomes dependent and withdrawn. This shift involves a switch in the γ-aminobutyric acid type A ($GABA_A$) receptors of VTA GABAergic neurons, from inhibitory to excitatory signaling.

The ventral tegmental area (VTA) serves as an anatomical locus controlling the switch from an opiate-nondependent to an opiate-dependent state (*1*, *2*). In nondependent rats, opiate reward is mediated by a dopamine-independent neural system, involving the brainstem tegmental pedunculopontine nucleus (TPP) (*3*). Once chronically exposed to opiates and in a state of withdrawal, opiate reward switches to a dopamine-dependent system (*3*). It has been observed that the switch between the two motivational systems is due to a switch in γ-aminobutyric acid type A ($GABA_A$) receptor functioning in VTA GABAergic neurons, from an inhibitory to an excitatory signaling state (fig. S1) (*2*).

Brain-derived neurotrophic factor (BDNF) is capable of producing this change in GABAergic response, from inhibitory to excitatory, as has been observed in the hippocampus during epileptic seizures (*4*) and in the spinal cord during neuropathic pain (*5*). BDNF is present in the VTA (*6*), and its TrkB receptors are present on both GABA (fig. S2) and dopamine VTA neurons (*7*, *8*). Chronic exposure to drugs of abuse increase BDNF levels in VTA neurons

[1]Department of Molecular Genetics, University of Toronto, 160 College Street, Toronto, Ontario M5S 3E1, Canada. [2]Institute of Medical Science, University of Toronto, 160 College Street, Toronto, Ontario M5S 3E1, Canada. [3]Department of Psychology, Brigham Young University, Provo, UT 84602, USA.

*To whom correspondence should be addressed. E-mail: vargashector@yahoo.com